ChemPubSoc Europe

DOI: 10.1002/cphc.201301083

Status of Dye Solar Cell Technology as a Guideline for Further Research

Andreas Hinsch,*[a] Welmoed Veurman,[a] Henning Brandt,[a] Katrine Flarup Jensen,[a] and Simone Mastroianni[a, b]

Recently, the first commercial dye solar cell (DSC) products based on the mesoscopic principle were successfully launched. Introduction to the market has been accompanied by a strong increase in patent applications in the field during the last four years, which is a good indication of further commercialization activity. Materials and cell concepts have been developed to such extent that easy uptake by industrial manufacturers is possible. The critical phase for broad market acceptance has therefore been reached, which implies focusing on standardization-related research topics. In parallel the number of scientific publications on DSC is growing further (>3500 since 2012), and the range of new or renewed fundamental topics is broadening. A recent example is the introduction of the perovskite mesoscopic cell, for which an efficiency of 14.1% has been certified. Thus, a growing divergence between market introduction and research could be the consequence. Herein, an attempt is made to show that such an unwanted divergence can be prevented, for example, by developing suitable reference-type cell and module concepts as well as manufacturing routes. An in situ cell manufacturing concept that can be applied to mesoscopic-based solar cells in a broader sense is proposed. As a guideline for future module concepts, recent results for large-area, glass-frit-sealed DSC modules from efficiency studies (6.6% active-area efficiency) and outdoor analysis are discussed. Electroluminescence measurements are introduced as a quality tool. Another important point that is addressed is sustainability, which affects both market introduction and the direction of fundamental research.

1. Introduction

1.1. Dye Solar Cell Technology

For 20 years, dye solar cell (DSC) technology has been the subject of much research and development and has received constant funding through international, European, and national research programs. The basic idea of DSCs being printable solar cells in which an organic-based dye is used as the photoactive compound has been very successfully verified. The highly interdisciplinary research that has been necessary is also reflected in the huge number of publications and patents (Figure 1).

Solar cell efficiencies of 12% for single cells[1] and 9.9% for smaller modules[2] have been reached in several laboratories, and further enhancement is predicted with progress in materials development. This has been shown with new material concepts in which the dye molecules have been replaced by perovskite nanocrystals, for which 14.1% efficiency was demonstrated recently.[3] Important benefits from the point of view of commercialization are the low investment costs, which allow for decentralized production, high sustainability, and a wide variety of product designs. Direct market competition with silicon solar cells is not seen at this stage.[4]

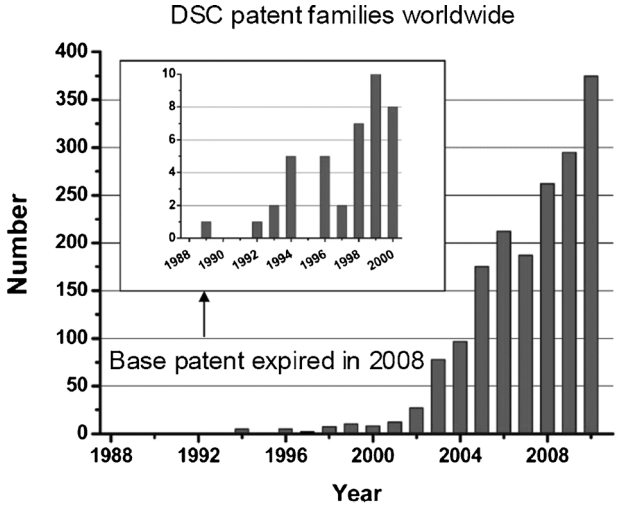

Figure 1. Yearly increase in DSC patent families worldwide, adopted from ref. [9].

1.2. DSC Technology Activities

Basic research on DSC is continuously carried out for materials optimization. The morphology of the nanocolloidal electrode layers is controlled, metal–organic and highly absorbing organ-

[a] Dr. A. Hinsch, W. Veurman, H. Brandt, K. Flarup Jensen, Dr. S. Mastroianni
Fraunhofer ISE
Heidenhofstraße 2
79110 Freiburg (Germany)
E-mail: andreas.hinsch@ise.fraunhofer.de

[b] Dr. S. Mastroianni
Freiburg Materials Research Centre (FMF)
Stefan-Meier Str. 21
79104 Freiburg (Germany)

ic dyes are developed, and various routes are followed for the transport of the photooxidized charges, such as molten-salt-based redox electrolytes and solid-state organic or hybrid hole conductors. In addition, various concepts for the cell setup are studied, for example, glass–glass-[5] and glass–monolithic-based concepts,[6] as well as flexible DSCs on metal[7] and plastic foils.[8] A lot of know-how has been built up in the characterization and understanding of both material and photoelectrochemical properties of DSC. Constant further development and the integration of new concepts for materials and cells are foreseen.

Applied research addresses the design and development of DSC modules; several interconnection concepts are followed, and sealing methods such as glass-frit sealing,[10] polymer sealing,[11] and laser sealing[12] have been implemented. Depending on the application, durability and accelerated aging tests such as light soaking, temperature cycling, and mechanical testing have been successfully established but still not developed to the level of standardization.[13] Prototyping of DSCs, which is done at institutes and companies, addresses and proves the upscalability of DSC modules, as well as flexibility in customized and decorative module design. Also first approaches towards system integration are undertaken.

For the commercial production of DSC, several pilot-plant lines have been installed or are under construction. A first full production line for flexible DSCs has been in operation since 2012. Specific production equipment is under constant development, and automation and quality control are addressed. Triggered by this development, several companies are increasingly working on the scaleup and quality control of materials for the key components of DSCs.

1.3. Market-Related DSC Activities

Due to the beneficial low-light performance of DSCs (>18% has been shown under indoor-light conditions),[14] the first attractive market for DSC products is consumer electronics, which goes together with the development of suitable electronics. A recent example is the successful introduction of flexible DSCs in the global lifestyle product market and a DSC-powered charger for cell phones (Figure 2).

A particular aspect of DSCs is the possibility for decentralized local production, which was realized in the early-stage market introduction of DSC modules for home solar systems and also for custom-made decorative DSC products. The recent success in scaling up of DSC modules on glass and foils demonstrates the suitability of DSC for the potentially very large building-integrated photovoltaics (BIPV) market, although a certification step is still required.

In particular, the combination with decorative architectural glass seems attractive (Figure 3), since it can exploit the large flexibility in transparency and colors of DSC devices for facade applications. In this case, besides the initial electrical characteristics of the device in terms of energy production, reliability of the facade throughout the lifetime of the device is mandatory. Electricity production and, more importantly, uniformity in the aesthetics of single cells and arrays of modules are pivotal for this kind of application, for which an expected lifetime of 20–25 years should be achieved.

Figure 2. Two recent examples of commercially available DSC-powered products: a flexible keyboard (top) and a battery charger for cell phones (bottom).

Figure 3. Showroom for BIPV applications of large-area, glass-frit-sealed DSC modules (meander type), as developed at Fraunhofer ISE (2012).

For certain types of roof elements a potential advantage of DSC lies in their design flexibility. Because of the demand from initial commercial DSC production, the market for DSC-specific materials is growing, and this increases the engagement of fine-chemical companies in the synthesis of nanomaterials, dyes, electrolytes, and organic hole conductors. With the setting up of DSC production, growing interest from machinery manufacturers will also be seen. There will be a demand for system integration for DSC from the electronics industry and the building-construction sector.

1.4. Reviews on DSC Research

Several detailed reviews have been written on DSC research in the past and the most recent are cited in the following. A broad thematic review is given in ref. [15]. A review focusing on the dye molecules and optimization of highly efficient DSCs

is given in ref. [16]. In a further review[17] new-generation materials and cell concepts are presented.

1.5. Results from a Survey of the Scientific Literature

For this paper a literature survey has been performed by using the Scopus database for peer-reviewed scientific literature on DSCs and perovskite solar cells as a new mesoscopic concept.[18] In the data range 1985 to present more than 11 000 documents (i.e. articles, conference papers, reviews) have been published on the topic of DSCs with a remarkable increasing trend in the very recent years (7000 papers in the past three years; see Figure 4a). Besides EPFL in Switzerland (388 publications, almost 3.5% of the total) and Uppsala University and KTH in Sweden (333 publications), the institutes and research groups that have made the largest contributions are located in Taiwan, Japan, Korea, and China (Table 1). The impressive exponential growth of publications on perovskite solar cells (Figure 4b) reflects the growing importance of this field in the last two years.

By focusing on the 20 most-cited papers in the years 2012 and 2013 it is possible to gain insight into the latest, most relevant research topics in the DSC field. This revealed that investigations of the optical and electrochemical characteristics of dyes for broadband absorption, increasing electron lifetime, and anti-aggregation properties of dye molecules occupy prominent positions.[1,19] In this context, several studies have a particular focus on porphyrin sensitizers. Secondly, TiO_2 with morphologies ranging from 1D nanostructures (nanowires and nanorod arrays) to 3D spheres (spherical aggregates, hollow spheres, core–shell particles) is extensively explored for the fabrication of photoanodes. A third area involves research on iodine-free redox couples (i.e. cobalt complexes, disulfide/thiolate) for achieving transparency and noncorrosive properties. Among these, new hole-transport materials for solid-state DSCs are also investigated. Finally, different catalytic materials are analyzed for better charge-transport mechanisms, higher performance, and economic benefits.

1.6. Development of Dyes

Many different classes of dyes have been tested and thoroughly optimized for DSCs, a selection of which is listed in Table 2. It can be expected that further modification of the dye molecular structure in combination with DFT calculations of the HOMO and LUMO electronic states will lead to a further increases in efficiency.[20]

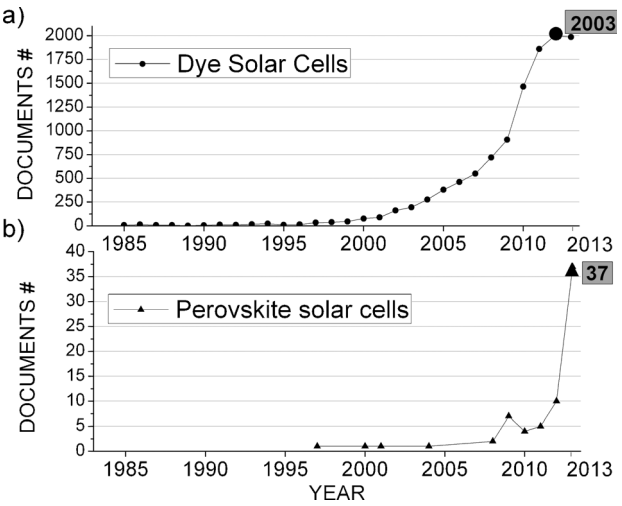

Figure 4. Number of scientific publications published per year in the field of DCSs (a) and perovskite solar cells (b). The values shown in the boxes are the maxima reached in 2012 for DSCs and in September 2013 for perovskite solar cells. Note that at the end of 2013 this value was 61. The literature search was performed by using the keywords "dye solar cell" and "perovskite solar cell" in the Scopus database.

1.7. Development of Redox Electrolytes

Electrolytes containing the I^-/I_3^- redox couple have been established as a standard since many years, and good stability data[24] have been reported for solvent-based and solvent-free (i.e. molten-salt-based) electrolytes, in particular in combination with ruthenium bipyridine dyes.[13] In addition, the combination with, for example, metal-free organic dyes such as the MK-type dyes has led to cells with long-term stability.[25] In first-generation DSCs the distance between photoelectrode

Table 1. Number of scientific publications published and relative percentage of the whole DSC literature from 1985 (ca. 11 000) produced by the leading 20 research institutes in the field. The literature search was performed by using the keyword "dye solar cell" in the Scopus database.

	Institute	Country	Publications	
1	Ecole Polytechnique Federale de Lausanne (EPFL)	Switzerland	388	3.48%
2	National Taiwan University	Taiwan	229	2.06%
3	National Institute of Advanced Industrial Science and Technology (AIST)	Japan	188	1.69%
4	Korea University	Korea	170	1.53%
5	Uppsala Universitet	Sweden	168	1.51%
6	The Royal Institute of Technology (KTH)	Sweden	165	1.48%
7	Korea Institute of Science and Technology (KIST)	Korea	163	1.46%
8	Dalian University of Technology (DUT)	China	161	1.45%
9	National University of Singapore	Singapore	156	1.40%
10	Imperial College London (ICL)	UK	139	1.25%
11	Seoul National University	Korea	138	1.24%
12	Pusan National University	Korea	136	1.22%
13	Huaqiao University	China	132	1.19%
14	Tsinghua University	China	132	1.19%
15	Institute of Plasma Physics Chinese Academy of Sciences	China	131	1.18%
16	Chinese Academy of Sciences	China	127	1.14%
17	Kyoto University	Japan	122	1.10%
18	Hanyang University	Korea	117	1.05%
19	Wuhan University	China	117	1.05%
20	Monash University	Australia	115	1.03%
72	Fraunhofer-Institut für Solare Energiesysteme	Germany	51	0.47%

Table 2. Examples of state-of-the-art efficiencies η achieved for different classes of dye molecules in DSC laboratory cells.

Color appearance in DSC	Type of dye	Laboratory	η [%][a]
red to dark brown	standard ruthenium metal–organic dye	EPFL	10.7
green to black	wide-band ruthenium metal–organic dye	Fujifilm, Sharp	11.9[21]
green to dark green	organic zinc porphyrin dye	EPFL	12.3[22]
blue to dark blue	organic donor–acceptor dye (donor–chromophore–anchor strategy)	Dongjin Semichem, EPFL	9.8[23]

[a] Measured with solvent-based electrolytes containing I^-/I_3^- or $[Co(bpy)_3]^{2+/3+}$ (bipy = 2,2′-bipyridine) as redox pair.

and counter electrode is rather large (typically 20 μm). This means that diffusion limitation of I_3^- can occur for operation under full-sun illumination. Therefore, the electrolyte must be highly doped with I_3^-, especially when more viscous molten-salt electrolytes are used. A typical "dark concentration" in this case is 0.1 M, which enhances electron recombination at the photoelectrode at high illumination. At low light illumination, this is not critical, because electrons trapped in states below the conduction band of TiO_2 only undergo slow recombination. Furthermore, it is important to increase the UV stability of these electrolytes by avoiding unwanted side reactions with photocatalytically formed OH radicals. Therefore, the water content of the electrolyte must be minimized.[26]

More recently, much work has focused on the optimization of highly soluble cobalt bipyridine and related redox complexes with the aim of lowering the oxidation potential towards the oxidized state of the dyes.[27] This has led to DSCs with photovoltages of up to 1 V, which is 250 mV higher than in the case of the I^-/I_3^- redox couple. The cobalt-based electrolytes are not compatible with ruthenium bipyridine dyes, because slow ligand exchange can be expected over time, but they are very suitable in combination with organic dyes.

1.8. Development of Counter Electrodes

Although a large effort is reported in the DSC literature for the effective replacement of transparent counter electrodes (CEs) activated by platinum nanoparticles, the latter are still the most widely used material for efficient and stable devices based on I^-/I_3^-. Alternative catalysts have been also investigated as CEs in combination with new redox couples such as disulfide/thiolate and Co_3^+/Co_2^+,[22,27,28] fo which platinum nanoparticles resulted in high charge-transfer resistance. Appropriate substitute catalysts for I^-/I_3^- reduction were found to be carbon materials (e.g. pure carbon black or mixtures thereof with graphite, graphene, or carbon nanotubes),[29] conductive organic polymers (e.g. polyaniline, PEDOT, PEDOT-TsO, or PEDOT-PSS), polymer–carbon composites,[29c] cobalt sulfide (CoS), and, more recently, $WO_{2.72}$, Fe_3O_4, mesoscopic vanadium carbide, and others.[29b] In particular, CEs in which vanadium carbide is embedded in mesoporous carbon showed catalytic activity similar to that of platinum nanoparticles.[29b]

1.9. Development of Photoactive Cathodes

Tandem solar cells fabricated by series/parallel connection of two separate devices (standard tandem architecture)[30] or dye-sensitizing both cell electrodes (integrated tandem architecture)[31] were investigated with the aim of increasing the overall device efficiency. Among the integrated tandem configurations, photoactive cathodes were proposed as a viable solution, and a maximum device efficiency of 2.4% was reached with an NiO photocathode.[32] Other p-type semiconductors (CuSCN,[33] CuO,[34] and, more recently, delafossites such as $CuGaO_2$[35] and $CuCrO_2$)[36] were also used as scaffolds for photoactive cathodes. Nevertheless, these materials did not perform better than NiO (and its doped form),[37] which remains the most investigated p-type metal oxide semiconductor.[38] Current issues for these materials are the position of the valence band (VB), which limits the open-circuit voltage V_{oc}, and the low hole mobility, which results in high charge-recombination rates and limits the thickness of the photocathode.

1.10. Development of Solid Organic Hole Conductors

With the aim of replacing the electrolyte in DSCs by an easily oxidizable solid hole conductor, several transparent organic p-type conductors have been studied (i.e. PEDOT,[39] P3HT,[40] and spiro-OMeTAD).[41] The most successful example is spiro-OMeTAD, which is also commercially available. This concept works best in combination with highly absorbing organic dyes of the donor–acceptor type, because the distance for diffusion of the electron hole to the back contact can be minimized to less than 5 μm in this case. Recently, p doping with Co^{III} complexes has also been demonstrated, and a maximum efficiency of 7.2% has been reached.[42]

1.11. Development of Inorganic Hole Conductors

Transparent inorganic materials have also been investigated for use as p-type conductors in DSCs.[43] Among these materials we can highlight CuI,[44] which reached efficiencies up to 4.7%,[45] and CuSCN,[15,46] which gave a maximum efficiency of 3.4%.[46c] Most of these p-type conductors have a tendency to form crystals, which leads to decreased regeneration of the oxidized dye molecules because of the large interfacial distance. Therefore, additives are often used to prevent crystallization.[47] On the contrary, enhancing of the p-type conductivity by, for example, replacing Cu^+ with triethylammonium has been shown.[46b]

Recently the inorganic perovskite $CsSnI_3$ has been successfully introduced as a p-type conductor in N719-sensitized solar cells. Surprisingly, this material with a 1.3 eV bandgap also contributed substantially to light sensitization. By doping $CsSnI_3$

with 5% of SnF_2, a device efficiency of 10% has been reported,[48] which can also be regarded as a first working example of a lead-free perovskite device. The p-type conductor CuSCN has also been applied in perovskite devices in order to fabricate fully inorganic solar cells with the aim of improving the device stability.[49]

1.12. Development of Organic–Inorganic Perovskites as New Types of Absorbers

Since the recent discovery[50] that the dye in DSCs can be replaced efficiently with metal–organic halide perovskite crystals, it became obvious that these soluble materials have very interesting properties for the realization of low-cost solar cells. In contrast to the molecular-dye sensitization concept, a high perovskite volume ratio of 50:50 relative to the mesoscopic TiO_2 is used. A certified cell efficiency of 14.1% was reached in 2013[51] and has triggered major research interest and started discussions on the underlying principles and the potential for improving the efficiency. An important finding is that, as the perovskite currently under study is a strong light absorber with an energy gap of 1.5 eV, the electrode spacing can be smaller than 0.5 μm and the p-selective contact at the back side can be achieved with an even thinner layer of less than 50 nm (see Table 3). The very narrow energy difference between the conduction band of the perovskite and that of TiO_2[52] should favor unwanted back-reactions, which, however, are seemingly not at all crucial in this case. It is therefore still not obvious whether a high inner surface contact to an electron-selective material like TiO_2 is beneficial or not. It can be predicted that classical-type thin-film solar cells with pure perovskite absorber material[53] will also attract increasing research interest, although the mesoscopic concept of filling a porous metal oxide layer with perovskites from solution has without doubt practical advantages.

Table 3. Summary of parameters for a recent mesoscopic perovskite cell made from the material $CH_3NH_3PbI_3$.[51]

Cell performance	I_{sc} [mA cm^{-2}]	V_{oc} [V]	FF	η [%]
	20.0	1.0	0.73	15
	E_{gap}[a] [eV]	VB [eV]	CB [eV]	Layer[b]
perovskite $CH_3NH_3PbI_3$	1.5	−5.4	−3.9	0.4 μm
mesoporous TiO_2	3.2	−7.2	−4.0	0.4 μm
dense TiO_2, "n contact"	3.2	–	–	< 30 nm
spiro-OMeTAD, "p contact"	–	–	−5.2	< 50 nm

[a] Bandgap. [b] TiO_2 as a 50:50 host for the perovskite.

1.13. Evaluation of Development Trends

In addition to the above discussion on efficiency developments for mesoporous devices, here a short evaluation of the current development of DSC technology with respect to stability and device concepts is given. Although stability is an important topic for introduction to the market and cells with long-term stability have been demonstrated,[54] only a small fraction of the scientific publications has focused on this field up to now. Moreover, results that are still controversial at first sight are reported. An example is the question whether water plays a stabilizing[55] or destabilizing role[56] in the thermal stability of devices. This was well clarified for stability testing in the presence of UV light, whereby water was shown to markedly accelerate cell degradation.[57] It can therefore be imagined that concepts like electrochemical pretreatment of the cell during manufacturing will lead to further stabilization of the device. An example is the electrochemical drying of ionic liquids.[58] On the other hand, it has also been shown that modification of the dye molecule by using a double-bond-edged Ru dye in combination with simple ionic liquid could lead to an important improvement in stability of a cell that withstood a 120 °C stress test for 480 h.[54b] For comparison purposes among different research groups, a complete device certification test is missing, since degradation stress tests are nowadays performed under different conditions of temperature, light intensity, uncontrolled humidity, working point of the cell (i.e. V_{oc}, short-circuit current I_{sc}, maximum power point P_{max}). These different procedures do not give straightforward comparable investigations and contribute to the increase in controversial results. Examples of applying such tests to DSCs have been reported.[13,59] Further points regarding the long-term stability of DSCs and that are in urgent need of development are the understanding of the importance of material purity for cell fabrication, the intrinsic evaluation of the material stability in the cell without considering the sealing effect, and the definition of a proper and comprehensive sealing procedure.

Many different device concepts have been developed up to now both for glass–glass cells and flexible substrates. As a general design rule, both long-term stability and manufacturability must be taken into account already at the research level. For effective cell development, module-related topics must be considered in the initial stage.[60] Two important topics are the minimization of the electrode distance for optimized charge transport, for example, in monolithic DSCs,[6] and properly sealed interconnections among cells to avoid electrophoresis due to the diffusion gradients of ions and protons under constant illumination.[61] Apart from choosing the right sealing procedure,[12,62] also modeling of the charge transport in a realistic cell is needed for better understanding of gradient-induced instabilities.[63]

Experimental Section

Details of Module Manufacturing at Fraunhofer ISE

The Fraunhofer ISE 60×100 cm^2 modules[5] and the small 10×10 cm^2 modules are manufactured with industry-relevant procedures and machines. Pilkington TEC-8, which is a 3.2 mm float glass coated with fluorine doped tin oxide (FTO), is used as substrate for the front and back electrodes. The glass substrates are cut mechanically to the proper size, and the filling holes at the back electrodes are drilled by laser, as is the structure in the transparent conductive oxide (TCO) layer in order to electrically insulate

the cells. After these preparation steps, the substrates are washed mechanically with demineralized water. Then all of the layers, including the glass-frit sealant and the ultrathin platinum back-electrode layer, are screen printed. Between each printing step, the layers are dried in a low-pressure step to remove bubbles followed by convection drying. The glass-frit sealant is a lead- and bismuth-free paste based on a $ZnO–SiO_2–Al_2O_3$ composition (Pröll KG, Germany).

For the catalytic back electrode a nanocolloidal platinum paste is used (3D-nano, Poland). Furthermore, for the TiO_2 layer and the silver contacts, commercially available pastes were purchased (Dyesol DSL 18 NR-T, Ferro lead-free silver paste). To burn out the organics from the printed pastes, the front and back electrodes are then sintered in an infrared oven. After the sintering step, the front and back electrodes are carefully positioned on top of each other and sealed tightly in a second furnace step at around 600 °C. For both steps common batch-size glass-fusing ovens are used, which heat the substrates by IR radiation from the top along with a thin graphite foil as an underlayer. No mechanical stress is applied during fusing. Figure 5 shows the temperature profiles for fusing

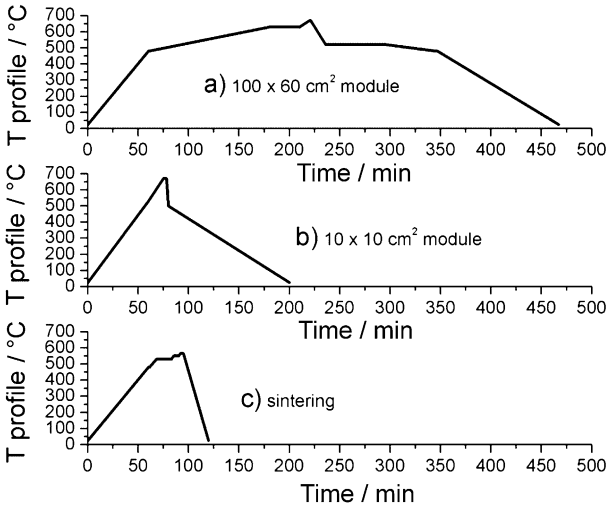

Figure 5. Glass-fusing temperature profiles for 100×60 cm (a) and 10×10 cm^2 (b) modules and sintering of the plates prior to fusing (c).

and sintering. The temperatures between 520 and 565 °C are related to the melting point of the glass frit. The fusing of the plates takes place well above the softening temperature of the TCO glass between 630 and 670 °C. The heat treatment below 520 °C is intended to achieve homogenous and stress-free heating and cooling of the glass. These *T* profiles are not optimized for industrial production.

When the oven steps are completed, the modules are colored through the filling holes. For applying the dye and the electrolyte, a customized, in-house development is used.[5] The filling device (Figure 6) consists of chemically inert tubing and valves made from Teflon. During the coloration process, the dye solution is pressed through the module by applying a constant gas pressure of 3 bar on the liquid reservoir. For the drying process nitrogen gas is purged through at a similar pressure. The electrolyte is first degassed by ultrasonication and then pressed into the module at 60–80 °C with a syringe pump. After filling and cooling, the holes are cleaned and sealed with a small piece of 0.3 mm thick glass. A high-power UV LED is used to cure the glue (Threebond).

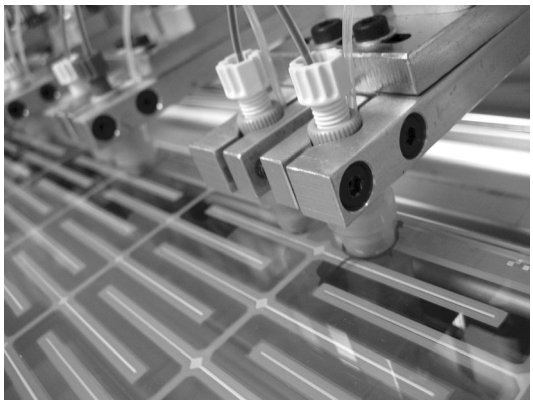

Figure 6. Customized, in-house-developed filling device to supply dye and electrolyte in an inert system to scaled-up DSC modules.

As a last step the electrical connections are soldered to the silver grid of the front and back electrodes by using an ultrasonic soldering device.

Preparing the Specialized 60×100 cm^2 Modules

A batch of 60 substrates of TCO glasses (30 front and 30 back electrodes) was prepared and screen-printed in an application laboratory. Afterwards all glasses were sintered, and the front and back electrodes were melted to each other in an IR oven. The fused modules have a plate distance of approximately 50 μm. Two modules from this batch were then prepared: one with a TiO_2 layer thickness of 12 μm for high-efficiency experiments (A) and one with a TiO_2 layer thickness of 8 μm for long-term outdoor measurements (B).

Module A was colored with 2.0 mM C101 dye[64] dissolved in pure DMSO. After the dying process acetonitrile was rinsed through the cells to remove residual dye solution. Then electrolyte was pumped into the module (0.6 M 1-methyl-3-propylimidazolium iodide, 25 mM I_2, 60 mM guanidine thiocyanate, and 0.3 M *N*-butylbenzimidazole in acetonitrile).

For module B a pure solution of 0.3 mM N719 dye in ethanol was used. After coloring, the module was dried by purging with nitrogen and then filled with a highly viscous, solvent-free electrolyte based on ionic liquids (Merck). With these materials a lower efficiency of approximately 2.5% on the active area resulted. The module was heated to 65 °C during the hole-sealing process to prevent later problems with thermal expansion. Afterwards, the finished module was glued to a UV-blocking hardened glass with a two-compound silicone epoxy (Wacker). By using a standard spacer frame the module was then totally encapsulated with a back glass, leaving out only the electrical contacts. The module was finally mounted on the roof of Fraunhofer ISE and equipped with a thermocouple for monitoring the temperature of the module.

Outdoor Tests

Outdoor tests on 60×100 cm^2 DSC modules were performed at Fraunhofer ISE in Summer 2013. The tilt angle of the module (45°) was set as the optimum for the summer season and for the latitude of Freiburg. The azimuth of the outdoor test stand on which the module was mounted was south. The module was operated continuously at the maximum power point (MPP) by means of

a suitable MPP tracker. Electrical and meteorological data were collected every 5 min.

Measurement of Electroluminescence, Cell Absorbance, and Photoluminescence

Electroluminescence imaging was performed on a 2.5 cm^2 cell and on a 100 cm^2 module. The module was forward-biased in the dark till a current equivalent to the I_{sc} under 1 sun illumination was reached. The current in this case was 0.42 A and the applied voltage was 1.59 V, 0.8 V per cell. The exposure time was 60 s. A silicon CCD detector with a long-pass filter with cutoff at 650 nm was used to detect the signal. The photoanode was directed towards the camera. Photoluminescence measurements were carried out under Ar laser excitation ($\lambda = 514.5$ nm, $E = 2.41$ eV) by using an Andor Shamrock 303i spectrometer equipped with an Si CCD cooled to $-95\,^{\circ}C$. The spectra were corrected for the spectral response of the instrument.[65] Absorbance spectra were obtained on a Varian Cary 5000 UV/Vis spectrophotometer.

2. Results and Discussion

2.1. Glass-Frit-Sealed DSC Modules

Recently, we demonstrated scale-up of dye-sensitized solar cells to large-area DSC modules prepared by glass-frit technology.[5] The modules were developed by using a meander and integrated series connection and reached a size of 6000 cm^2. In this work, prototypes were now produced in a more stable industrial environment. A batch of 60 substrates was screen-printed. Optimized screen-printing and drying processes were applied, as well as improved handling of the chemistry. With the aim of demonstrating high efficiency, a combination of C101 dye and an acetonitrile-based electrolyte was applied. An active-area efficiency of 6.6% and a total-area efficiency of 3.2% under 1 sun illumination (class B constant illumination at a module temperature of 45 °C) was reached (module A). Figure 7 shows the performance of such a module. These values could relatively easily be improved in the near future. The non-active area of 46% in these module prototypes is still too high. In a next step, achieving 20% non-active area by printing of thinner glass-frit lines is a realistic goal. Moreover, the series resistance caused by the contacts and the catalytic function of the back electrode limit the fill factor (FF). Assuming an FF of 70%, the active-area efficiency would then be 8.8%. If this could be combined with a non-active area of 20%, a module efficiency of 7% would be within reach.

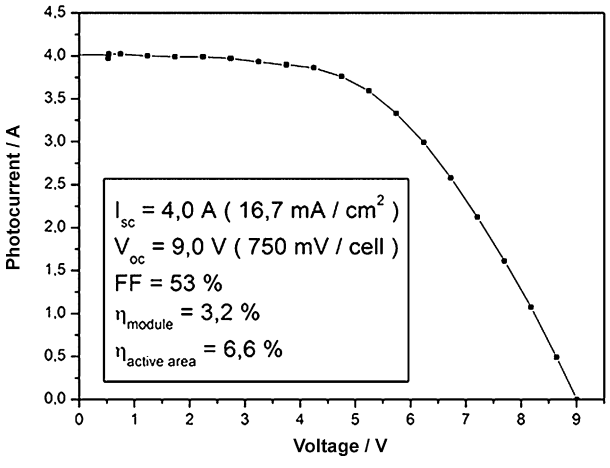

Figure 7. Current–voltage characteristics for a large, highly efficient 6000 cm^2 module.

2.2. Monitoring Outdoor Module Stability

Continuous outdoor monitoring was performed on the 100 × 60 cm^2 module B. The trend of the maximum power point P_{max} at 1000 $W\,m^{-2}$ of irradiation on the module plane is shown in Figure 8 over the first 100 days of exposure. The P_{max} values were obtained through polynomial fitting of the P_{max} versus irradiance curve for sunny days and extracting the value at 1000 $W\,m^{-2}$. The influence of meteorological parameters such as module temperature, wind speed, and the angle of incidence of the solar rays was not taken into account.[66] However, only a small deviation in these parameters can be expected, since the measurements were performed during the same season, and thus the behavior of the module can be considered to be reliable and close to reality. After a small increase in P_{max} of 1.5% over the first ten days or so of outdoor exposure, a small constant decrease was observed, after which apparent stabilization was reached in the final period. The P_{max} decay after 100 days was less than 11%.

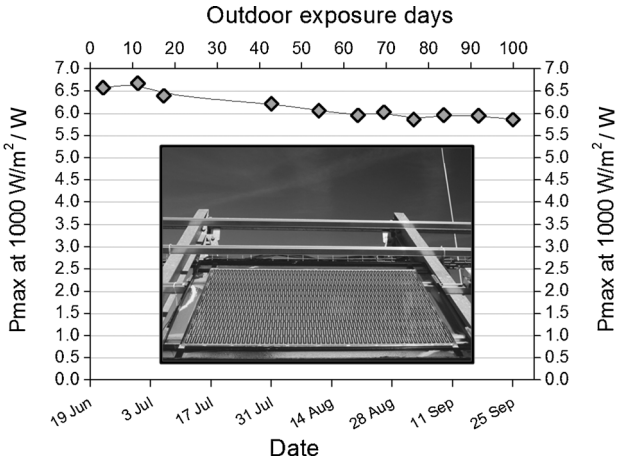

Figure 8. Trend of P_{max} at 1000 $W\,m^{-2}$ of irradiation on the module plane over 100 days of outdoor exposure (Summer season). The line connecting the P_{max} points is a guide to the eye. The inset shows the 100 × 60 cm^2 module mounted on the ISE rooftop stand (tilt = 45 °C, azimuth South).

To better analyze the outdoor behavior of the module, Figure 9a shows a plot of P_{max} versus irradiation on the module plane after 5 days of module exposure (June 22) and after 100 days (September 25). Interestingly, the P_{max} deviation between the two trends up to 400 $W\,m^{-2}$ remains rather small. The reasons for the 11% decrease in P_{max} at 1000 $W\,m^{-2}$ after 100 days can be analyzed through Figure 9b, in which voltage V_{max} and current I_{max} at P_{max} are plotted. After 100 days V_{max} de-

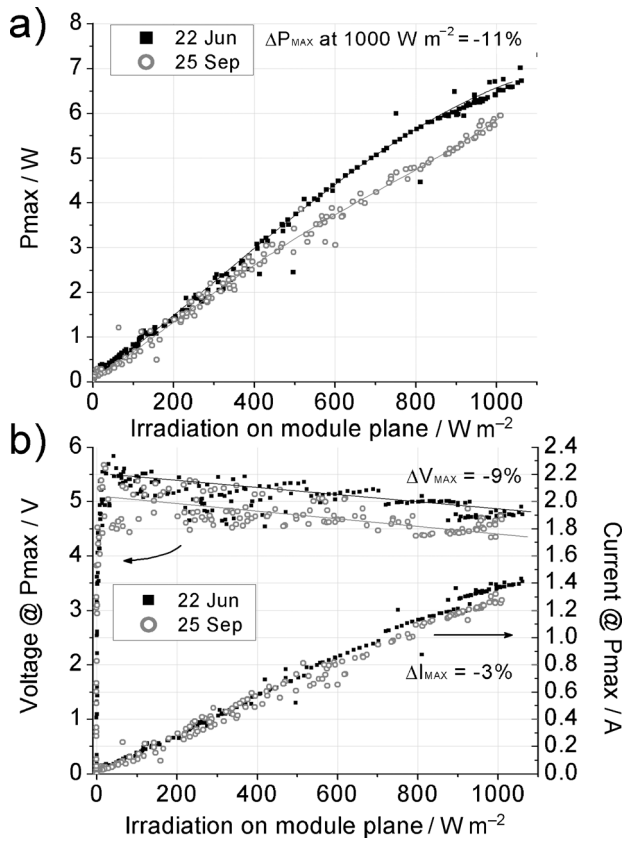

Figure 9. a) P_{max} and b) V_{max} and I_{max} at P_{max} plotted versus irradiation on the module plane after 5 days of outdoor module exposure (June 22) and after 100 days (September 25). The variations in P_{max}, V_{max}, and I_{max} show the decrease in electrical performance that occurred in 100 d. Solid lines in a) and b) show polynomial and linear fittings performed for P_{max} and V_{max}, respectively.

creased by 9%, but I_{max} dropped by only 3%, which indicates a negligible decrease in I_{sc}. Hence, the decrease in V_{oc} with time, along with a possible increase in series resistances, plays the main role in the loss of module performance.[63b]

2.3. Electroluminescence as a New Quality Tool for DSCs

Electroluminescence (EL) is a well-known and fast inspection tool for silicon PV technologies to study shunts, non-active areas, and effects of serial resistances. Since the works by Trupke, Würfel et al. in 1999 and 2000,[67] only recently was EL systematically investigated on laboratory-scale DSCs as a spatial characterization technique for analyzing aging effects.[68] In this section we give evidence that this technique can profitably be applied to large-area modules as well.

The EL signal results from radiative recombination of electrons from the LUMO with the holes present in the HOMO of the dye, and it is generated under sufficiently high forward bias. Under these conditions, electrons are injected at the photoanode from the TCO to the TiO_2 conduction band (CB) and from here to the LUMO of the dye, generating an excited state in the sensitizer. To give rise to radiative recombinations (and thus to the EL signal), dye oxidation by the oxidizing I_3^- ions in the electrolyte must occur at the HOMO level. Therefore, it can be hypothesized that the intensity of the electroluminescence signal is a function of the amount and type of active dye molecules adsorbed on the TiO_2 and the local current density in the cell, which also depends on electron recombination at the TiO_2/electrolyte interface and on the I_3^- concentration, as well as being a measure of the quasi-Fermi-level splitting, since EL generation involves electron injection from the density of states of the TiO_2 CB into the LUMO.[67b,69]

To investigate the influence of the amount of dye molecules on the EL signal in a large-area cell, a 5 cm-long glass-sealed DSC was fabricated with a dye-flushing time of 180 s (Figure 10a). The non-uniformity of the dye coverage can be clearly observed in the photograph of the cell. The EL image in Figure 10b strongly matches the distribution of dye molecules in the cell, with a significant contribution close to the sensitizer filling hole and a gradual decrease towards the second hole. A more accurate picture is given by the EL intensity profile scanned across the length L of the cell (Figure 10c), which shows an initial dominant peak and the consequent absence

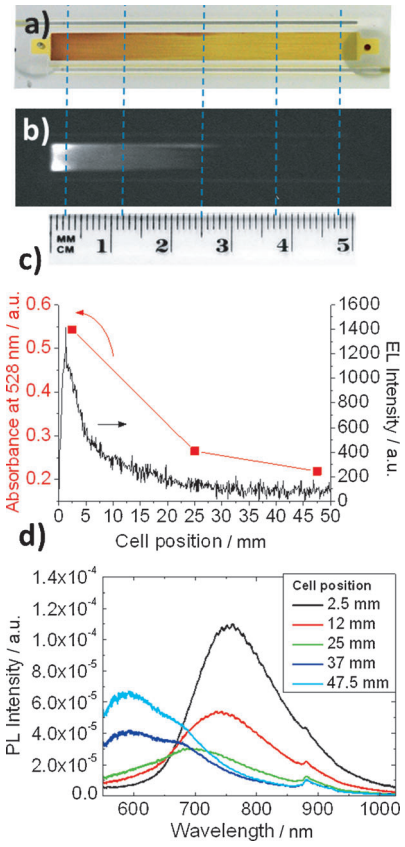

Figure 10. a) Photograph of a complete 5 cm-long DSC fabricated with a dye-flushing time of 180 s. The color gradient in the cell clearly shows that the dye filling hole is on the left side of the cell. b) EL imaging of the same cell. c) Absorbance peak at 528 nm and EL intensity profile scanned across the length of the cell. Lines connecting symbols of the absorbance are guides to the eye. d) PL intensity measured on five spots at regular intervals on the same cell. Dashed lines crossing a) and b) correspond to the cell areas where EL, absorbance, and PL were measured.

of signal for $L \gtrsim 30$ mm. In the same plot the absorbance peaks measured at 528 nm for three different L values are also shown. At $L = 25$ mm (center of the cell) the absorbance peak has only a very small contribution of the dye spectrum, whereas at $L = 47.5$ mm it is due exclusively to the glass/TCO, the Pt, and the absorption tail of the electrolyte.

With the aim of gaining more insight, Figure 10d shows photoluminescence (PL) spectra recorded at five different L values. In the areas where relatively large amounts of dye molecules are present ($L \approx 2.5$ mm) the dye emission peak is centered at 760 nm, whereas for larger L an additional PL signal appears at shorter wavelengths. For isolated molecules the dye emission peak has been ascribed to a phosphorescence signal stemming from radiative relaxations between the first excited triplet state of the dye and its ground state (the HOMO).[69,70] Nevertheless, in our case weakly adsorbed dye molecules should not be present, since the TiO_2 surface is only partially covered with dye because of the very short flushing time. For larger L values the dye peak decreases and an additional PL signal appears at shorter wavelengths. This probably arises from a fluorescence contribution of the electrolyte, which is quenched by the presence of the dye. This fluorescence can, in fact, be observed for $L = 37$ mm and $L = 47.5$ mm, where no dye molecules are present on the TiO_2 surface.

The trend in the absorption at 528 nm, the PL intensity at 760 nm, and the EL signal profile confirms that the observed electroluminescence originates from the dye molecules. Although further analysis is necessary, a combination of PL and EL imaging should also be regarded as a further possible technique for analyzing spatial variations in DSCs.

The information acquired through the above analysis can be applied to a 10×10 cm^2 DSC module. Figure 11 shows the image of the EL intensity map. The homogeneity of the luminescence indicates that the TiO_2 layer does not show manufacturing irregularities or poor adhesion to the TCO electrode. Some areas show a gradual decrease in signal intensity caused by an inhomogeneous coloring process. Also, areas that are not covered by the electrolyte owing to insufficient filling with electrolyte can be seen clearly.

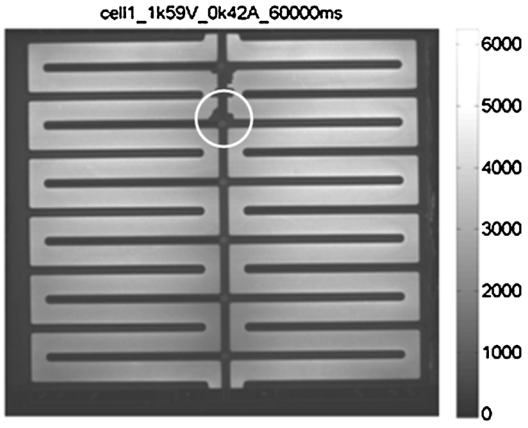

Figure 11. EL image of a 100 cm^2 module showing a mostly homogenous coloration. The circle indicates non-active areas due to insufficient electrolyte filling.

2.4. Homogenous Minimization of Electrode Distance in Glass-Frit-Sealed Modules

Since interest in perovskite-cell technology is strongly growing, it is necessary to research how to scale up the cell in an economical way. We investigated using the standard glass-frit DSC setup for this purpose. Due to the ultrathin carrier layers of the active materials in the perovskite cell, it is a necessary first step to minimize the electrode distance of the glass-frit setup and to equip it with a range of process-supporting optimizations. A batch of experimental plates (7.5×10 cm) was screen-printed, sintered, and fused to investigate the possible minimization of the distance between the counter and working electrodes. Therefore, the glass-frit paste and the TiO_2 paste were diluted by a factor of ten and the temperature profiles of the IR oven were optimized similarly to those shown in Figure 5. As an intermediate result, the distance was reproducibly minimized to 2 μm, as shown by scanning electron microscopy (Figure 12).

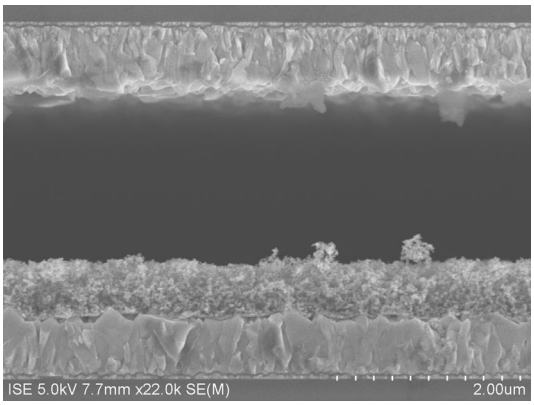

Figure 12. SEM cross-section image of a glass-frit-sealed cell with minimized layer thickness showing the spacing between the TCO electrodes (1.8 μm). This spacing was homogenously measured throughout the cell width (6 mm). The mesoporous TiO_2 (0.6 μm) and TCO (0.7 μm) layers are visible.

3. Conclusion

3.1. DSC Research and Technology

Recently, the first commercial DSC products based on the mesoscopic principle were successfully launched. Market introduction was accompanied by a strong increase in patent applications in this field during the last four years, which is a good indication of further commercialization activities. Materials and cell concepts have been developed to such an extent that easy uptake by industrial manufacturers is possible. The critical phase for broad market acceptance has therefore been reached, which suggests focusing on standardization-related research topics such as electroluminescence. In parallel, the number of scientific publications on DSC is growing further (>3500 since 2012) and the range of new or renewed fundamental topics is broadening. A recent example is the introduction of the perovskite mesoscopic cell, for which an efficiency

of 14.1% has been certified. Thus, a growing divergence between market introduction and research could be the consequence.

3.2. In Situ Manufacturing Concept for Mesoscopic Solar Cells

With the aim of preventing growing divergence between market introduction and broadening of scientific concepts, we have proposed an in situ cell-manufacturing concept that can be applied to mesoscopic-based solar cells in a wider sense. On the basis of our previous experience with glass-frit-sealed DSCs, a procedure is proposed wherein the screen-printed mesoscopic carrier layers are sequentially flushed with dissolved active materials through a specifically arranged groove into the glass-frit-sealed cell. The groove transports the solutions along the cell lengths, whereas the porous layers pull liquids by capillary forces into the cell width. By varying the porosities and particle sizes in the layer structure the dissolved active materials (absorber and p-type conductor) are guided to their destinations in a self-organizing process (see Figure 13 for the in situ cell concept). Subsequent thermal treatments and pressure/vacuum operations support this procedure. The encapsulation and in situ formation of the PV-active materials are in this case combined in a cost-effective and sustainable process (Figure 14).

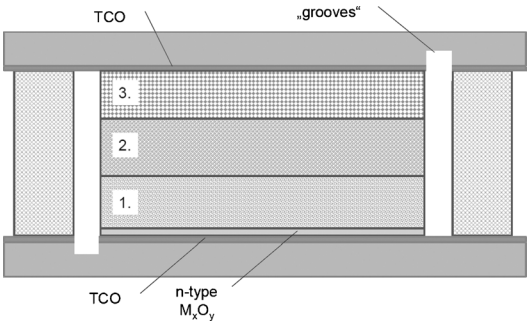

Figure 13. Generalized in situ cell concept for the scaleup of sealed mesoscopic solar cells as proposed by the authors in 2013. The mesoscopic inorganic layers 1–3 have different porosities and particle sizes; this allows in situ sequential wet-chemical deposition of the active materials through capillary forces. Filling and drying is facilitated through grooves in the glass.

3.3. Sustainability

Important factors to judge the sustainability of photovoltaic modules are the carbon footprint and the availability of materials. A detailed life-cycle assessment requires in-depth investigation and must be accounted for in further optimization. In the framework of this paper, only a brief calculation of the carbon footprint can be made. Following the above-described manufacturing process, more than 99.5% of the module material consists of recyclable glass and no additional lamination foils are required. By assuming a factor of 1.5 of additional energy consumption for the sintering and fusing steps, the energy balance is comparable to that of the production of flat glass. Thus, a very low carbon footprint number of 16 g of CO_2 per photovoltaically generated kilowatt hour results,[71] assuming a PV module efficiency of 12–14% (single junction), which is a realistic mid-term target after the recent progress in dye and especially perovskite development, as well as an operating time of 25 years.

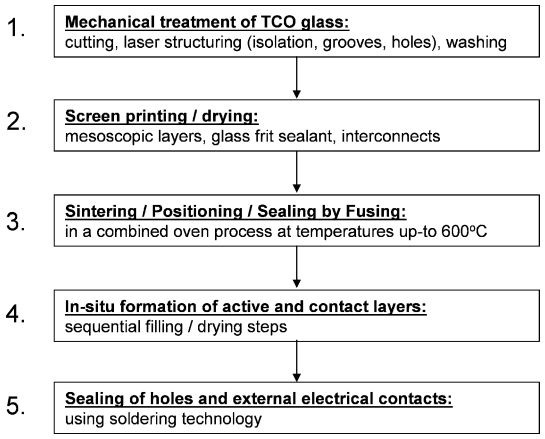

Figure 14. Basic production steps, developed by Fraunhofer ISE, which are related to the manufacturing of glass-frit-sealed DSCs or mesoscopic solar cell modules in the thematically broader sense. The encapsulation and in situ formation of the PV active layers are combined in a cost-effective and sustainable process.

The amount of active materials in DSC is low, although for the first-generation materials (0.1 g m^{-2} Ru, 0.02 g m^{-2} Pt, and 1–3 g m^{-2} I_2) availability for larger production volumes may be limited. The next-generation materials such as metal-free organic dyes, cobalt-complex redox electrolytes (0.5 g Co/m^2), organic hole conductors, and non-precious-metal organohalide perovskites ($<$0.2 g m^{-2} of Pb, Sn, Bi, Fe, etc. and 0.3 g m^{-2} I_2) will have virtually no limitations of availability. For cobalt and lead the environmental impact (critical concentration in soils is approximately 0.1 g kg^{-1} soil for both metals) must also be taken into account if modules are broken and eventually leached out by rain. In comparison, the values for these metals are still a factor of 100 less critical than that of cadmium.

Acknowledgements

This work was partially supported by the Foundation of Baden-Württemberg under project FSZ-Initiative. We would like to thank the following colleagues at Fraunhofer ISE for experimental assistance: Stefan Brachmann for performing the outdoor measurements, Elizabeth Schaeffer for absorbance measurements, Laura Mundt, Jens Peter Reinhardt and Manuel Schnabel for electroluminescence and photoluminescence data, and Jutta Zielonka for recording SEM images. In addition we would like to thank the company Thieme, Teningen Germany, for screen printing of DSC modules. K.F.J. thanks Konkuk University, Seoul, Korea, for financial support.

Keywords: dyes/pigments · electrochemistry · mesoscopic principle · photochemistry · solar cells

[1] L.-L. Li, E. W.-G. Diau, *Chem. Soc. Rev.* **2013**, *42*, 291 – 304.
[2] M. Morooka, R. Ogura, M. Orihashi, M. Takenaka, *Electrochemistry* **2009**, *77*, 960 – 965.
[3] M. A. Green, K. Emery, Y. Hishikawa, W. Warta, E. D. Dunlop, *Prog. Photovoltaics* **2013**, *21*, 1 – 11.
[4] Parts of this work have been published already in a proceedings paper: A. Hinsch, *Proceedings of the 28th European Photovoltaic Solar Energy Conference and Exhibition*, Paris, **2013**, 2239 – 2247
[5] A. Hinsch, W. Veurman, H. Brandt, R. L. Aguirre, K. Bialecka, K. F. Jensen, *Prog. Photovoltaics* **2012**, *20*, 698 – 710.
[6] H. Pettersson, T. Gruszecki, C. Schnetz, M. Streit, Y. Xu, L. Sun, M. Gorlov, L. Kloo, G. Boschloo, L. Häggman, A. Hagfeldt, *Prog. Photovoltaics* **2010**, *18*, 340 – 345.
[7] G. Hashmi, K. Miettunen, T. Peltola, J. Halme, I. Asghar, K. Aitola, M. Toivola, P. Lund, *Renewable Sustainable Energy Rev.* **2011**, *15*, 3717 – 3732.
[8] K. Miettunen, J. Halme, P. Lund, *Wiley Interdiscip. Rev.: Energy Environ.* **2013**, *2*, 104 – 120.
[9] H. Pettersson, K. Nonomura, L. Kloo, A. Hagfeldt, *Energy Environ. Sci.* **2012**, *5*, 7376 – 7380.
[10] a) A. Hinsch, U. Belledin, H. Brandt, F. Einsele, S. Hemming, D. Koch, U. Rau, R. Sastrawan, T. Schauer, *Proceedings of the IEEE Fourth World Conference on Photovoltaic Energy Conversion*, **2006**; b) R. Sastrawan, J. Beier, U. Belledin, S. Hemming, A. Hinsch, R. Kern, C. Vetter, F. M. Petrat, A. Prodi-Schwab, P. Lechner, W. Hoffmann, *Sol. Energy Mater. Sol. Cells* **2006**, *90*, 1680 – 1691.
[11] S. Noda, K. Nagano, E. Inoue, T. Egi, T. Nakashima, N. Imawaka, M. Kanayama, S. Iwata, K. Toshima, K. Nakada, K. Yoshino, *Synth. Met.* **2009**, *159*, 2355 – 2357.
[12] F. Ribeiro, J. MaçAira, R. Cruz, J. Gabriel, L. Andrade, A. Mendes, *Sol. Energy Mater. Sol. Cells* **2012**, *96*, 43 – 49.
[13] J. M. Kroon, N. J. Bakker, H. J. P. Smit, P. Liska, K. R. Thampi, P. Wang, S. M. Zakeeruddin, M. Grätzel, A. Hinsch, S. Hore, U. Würfe, R. Sastrawan, J. R. Durrant, E. Palomares, H. Pettersson, T. Gruszecki, J. Walter, K. Skupien, G. E. Tulloch, *Prog. Photovoltaics* **2007**, *15*, 1 – 18.
[14] Fujikura news report: http://www.fujikura.co.jp/eng/f-news/2035577_4207.html, **2012**.
[15] A. Hagfeldt, G. Boschloo, L. Sun, L. Kloo, H. Pettersson, *Chem. Rev.* **2010**, *110*, 6595 – 6663.
[16] S. Zhang, X. Yang, Y. Numata, L. Han, *Energy Environ. Sci.* **2013**, *6*, 1443 – 1464.
[17] B. E. Hardin, H. J. Snaith, M. D. McGehee, *Nat. Photonics* **2012**, *6*, 162 – 169.
[18] Scopus DSC literature survey: http://scopus.com, **2013**.
[19] a) L. Han, A. Islam, H. Chen, C. Malapaka, B. Chiranjeevi, S. Zhang, X. Yang, M. Yanagida, *Energy Environ. Sci.* **2012**, *5*, 6057 – 6060; b) S. Haid, M. Marszalek, A. Mishra, M. Wielopolski, J. Teuscher, J.-E. Moser, R. Humphry-Baker, S. M. Zakeeruddin, M. Grätzel, P. Bäuerle, *Adv. Funct. Mater.* **2012**, *22*, 1291 – 1302; c) Y.-S. Yen, H.-H. Chou, Y.-C. Chen, C.-Y. Hsu, J. T. Lin, *J. Mater. Chem.* **2012**, *22*, 8734 – 8747; d) W. Zou, C. Visser, J. A. Maduro, M. S. Pshenichnikov, J. C. Hummelen, *Nat. Photonics* **2012**, *6*, 560 – 564.
[20] M. Pastore, E. Mosconi, F. De Angelis, M. Grätzel, *J. Phys. Chem. C* **2010**, *114*, 7205 – 7212.
[21] Source Sharp cooperation certified by AIST in 2013, designed area 1.00 cm^2.
[22] A. Yella, H.-W. Lee, H. N. Tsao, C. Yi, A. K. Chandiran, M. K. Nazeeruddin, E. W.-G. Diau, C.-Y. Yeh, S. M. Zakeeruddin, M. Grätzel, *Science* **2011**, *334*, 629 – 634.
[23] J.-H. Yum, T. W. Holcombe, Y. Kim, K. Rakstys, T. Moehl, J. Teuscher, J. H. Delcamp, M. K. Nazeeruddin, M. Grätzel, *Sci. Rep.* **2013**, *3*, 2446.
[24] a) N. Jiang, T. Sumitomo, T. Lee, A. Pellaroque, O. Bellon, D. Milliken, H. Desilvestro, *Sol. Energy Mater. Sol. Cells* **2013**, *119*, 36 – 50; b) A. Hinsch, J. M. Kroon, R. Kern, I. Uhlendorf, J. Holzbock, A. Meyer, J. Ferber, *Prog. Photovoltaics* **2001**, *9*, 425 – 438.
[25] K. Hara, Z.-S. Wang, Y. Cui, A. Furube, N. Koumura, *Energy Environ. Sci.* **2009**, *2*, 1109 – 1114.
[26] K. F. Jensen, W. Veurman, H. Brandt, C. Im, J. Wilde, A. Hinsch, *MRS Online Proceedings Library,* **2013**, *1537*, mrss13-1537-b11-14.
[27] S. M. Feldt, E. A. Gibson, E. Gabrielsson, L. Sun, G. Boschloo, A. Hagfeldt, *J. Am. Chem. Soc.* **2010**, *132*, 16714 – 16724.
[28] M. Wang, N. Chamberland, L. Breau, J.-E. Moser, R. Humphry-Baker, B. Marsan, S. M. Zakeeruddin, M. Grätzel, *Nat. Chem.* **2010**, *2*, 385 – 389.
[29] a) M. Wu, X. Lin, T. Wang, J. Qiu, T. Ma, *Energy Environ. Sci.* **2011**, *4*, 2308 – 2315; b) M. Wu, X. Lin, Y. Wang, L. Wang, W. Guo, D. Qi, X. Peng, A. Hagfeldt, M. Grätzel, T. Ma, *J. Am. Chem. Soc.* **2012**, *134*, 3419 – 3428; c) T. N. Murakami, M. Grätzel, *Inorg. Chim. Acta* **2008**, *361*, 572 – 580.
[30] M. Yanagida, N. Onozawa-Komatsuzaki, M. Kurashige, K. Sayama, H. Sugihara, *Sol. Energy Mater. Sol. Cells* **2010**, *94*, 297 – 302.
[31] a) R. Tagliaferro, D. Gentilini, S. Mastroianni, A. Zampetti, A. Gagliardi, T. M. Brown, A. Reale, A. Di Carlo, *RSC Adv.* **2013**, *3*, 20273 – 20280.
[32] A. Nattestad, A. J. Mozer, M. K. Fischer, Y.-B. Cheng, A. Mishra, P. Bäuerle, U. Bach, *Nat. Mater.* **2010**, *9*, 31 – 35.
[33] K. Tennakone, A. Kumarasinghe, P. Sirimanne, G. Kumara, *Thin Solid Films* **1995**, *261*, 307 – 310.
[34] S. Sumikura, S. Mori, S. Shimizu, H. Usami, E. Suzuki, *J. Photochem. Photobiol. A* **2008**, *194*, 143 – 147.
[35] a) M. Yu, G. Natu, Z. Ji, Y. Wu, *J. Phys. Chem. Lett.* **2012**, *3*, 1074 – 1078; b) A. Renaud, B. Chavillon, L. Le Pleux, Y. Pellegrin, E. Blart, M. Boujtita, T. Pauporté, L. Cario, S. Jobic, F. Odobel, *J. Mater. Chem.* **2012**, *22*, 14353 – 14356.
[36] D. Xiong, Z. Xu, X. Zeng, W. Zhang, W. Chen, X. Xu, M. Wang, Y.-B. Cheng, *J. Mater. Chem.* **2012**, *22*, 24760 – 24768.
[37] a) G. Natu, P. Hasin, Z. Huang, Z. Ji, M. He, Y. Wu, *ACS Appl. Mater. Interfaces* **2012**, *4*, 5922 – 5929; b) H. Yang, G. H. Guai, C. Guo, Q. Song, S. P. Jiang, Y. Wang, W. Zhang, C. M. Li, *J. Phys. Chem. C* **2011**, *115*, 12209 – 12215.
[38] a) F. Odobel, Y. Pellegrin, E. A. Gibson, A. Hagfeldt, A. L. Smeigh, L. Hammarström, *Coord. Chem. Rev.* **2012**, *256*, 2414 – 2423; b) F. Odobel, L. c. Le Pleux, Y. Pellegrin, E. Blart, *Acc. Chem. Res.* **2010**, *43*, 1063 – 1071; c) F. Odobel, Y. Pellegrin, *J. Phys. Chem. Lett.* **2013**, *4*, 2551 – 2564.
[39] Y. Saito, T. Kitamura, Y. Wada, S. Yanagida, *Synth. Met.* **2002**, *131*, 185 – 187.
[40] a) P. Ravirajan, A. M. Peiró, M. K. Nazeeruddin, M. Graetzel, D. D. C. Bradley, J. R. Durrant, J. Nelson, *J. Phys. Chem. B* **2006**, *110*, 7635 – 7639; b) K. J. Jiang, K. Manseki, Y. H. Yu, N. Masaki, K. Suzuki, Y. L. Song, S. Yanagida, *Adv. Funct. Mater.* **2009**, *19*, 2481 – 2485.
[41] U. Bach, D. Lupo, P. Comte, J. E. Moser, F. Weissörtel, J. Salbeck, H. Spreitzer, M. Grätzel, *Nature* **1998**, *395*, 583 – 585.
[42] J. Burschka, A. Dualeh, F. Kessler, E. Baranoff, N.-L. Cevey-Ha, C. Yi, M. K. Nazeeruddin, M. Grätzel, *J. Am. Chem. Soc.* **2011**, *133*, 18042 – 18045.
[43] B. Li, L. Wang, B. Kang, P. Wang, Y. Qiu, *Sol. Energy Mater. Sol. Cells* **2006**, *90*, 549 – 573.
[44] a) Q. B. Meng, K. Takahashi, X. T. Zhang, I. Sutanto, T. N. Rao, O. Sato, A. Fujishima, H. Watanabe, T. Nakamori, M. Uragami, *Langmuir* **2003**, *19*, 3572 – 3574; b) G. Kumara, S. Kaneko, M. Okuya, K. Tennakone, *Langmuir* **2002**, *18*, 10493 – 10495; c) K. Tennakone, G. Kumara, I. Kottegoda, K. Wijayantha, V. Perera, *J. Phys. D* **1998**, *31*, 1492.
[45] G. Kumara, M. Okuya, K. Murakami, S. Kaneko, V. Jayaweera, K. Tennakone, *J. Photochem. Photobiol. A* **2004**, *164*, 183 – 185.
[46] a) G. Larramona, C. Choné, A. Jacob, D. Sakakura, B. Delatouche, D. Péré, X. Cieren, M. Nagino, R. Bayón, *Chem. Mater.* **2006**, *18*, 1688 – 1696; b) E. Premalal, G. Kumara, R. Rajapakse, M. Shimomura, K. Murakami, A. Konno, *Chem. Commun.* **2010**, *46*, 3360 – 3362; c) E. Premalal, N. Dematage, G. Kumara, R. Rajapakse, M. Shimomura, K. Murakami, A. Konno, *J. Power Sources* **2012**, *203*, 288 – 296.
[47] A. Konno, T. Kitagawa, H. Kida, G. A. Kumara, K. Tennakone, *Curr. Appl. Phys.* **2005**, *5*, 149 – 151.
[48] I. Chung, B. Lee, J. He, R. P. Chang, M. G. Kanatzidis, *Nature* **2012**, *485*, 486 – 489.
[49] S. Ito, S. Tanaka, H. Vahlman, H. Nishino, K. Manabe, P. Lund, *ChemPhysChem* **2013**, DOI: 10.1002/cphc.201301047
[50] M. M. Lee, J. Teuscher, T. Miyasaka, T. N. Murakami, H. J. Snaith, *Science* **2012**, *338*, 643 – 647.
[51] J. Burschka, N. Pellet, S.-J. Moon, R. Humphry-Baker, P. Gao, M. K. Nazeeruddin, M. Gratzel, *Nature* **2013**, *499*, 316 – 319.

[52] H. S. Kim, C. R. Lee, J. H. Im, K. B. Lee, T. Moehl, A. Marchioro, S. J. Moon, R. Humphry-Baker, J. H. Yum, J. E. Moser, M. Grätzel, N. G. Park, *Sci. Rep.* **2012**, *2*, 591.
[53] M. Liu, M. B. Johnston, H. J. Snaith, *Nature* **2013**, *501*, 395 – 398.
[54] a) M. Marszalek, F. D. Arendse, J. D. Decoppet, S. S. Babkair, A. A. Ansari, S. S. Habib, M. Wang, S. M. Zakeeruddin, M. Grätzel, *Adv. Energy Mater.* **2013**, DOI: 10.1002/aenm.201301235; b) S. Ito, K. Takahashi, S.-i. Yusa, M. Saito, T. Shigetomi, *Int. J. Photoenergy* **2013**, 9.
[55] a) C. Law, S. C. Pathirana, X. Li, A. Y. Anderson, P. R. F. Barnes, A. Listorti, T. H. Ghaddar, B. C. Oregan, *Adv. Mater.* **2010**, *22*, 4505 – 4509; b) K. Zhu, S. R. Jang, A. J. Frank, *Energy Environ. Sci.* **2012**, *5*, 9492 – 9495.
[56] a) M. Sumita, K. Sodeyama, L. Han, Y. Tateyama, *J. Phys. Chem. C* **2011**, *115*, 19849 – 19855; b) M. Hahlin, E. M. J. Johansson, R. Schölin, H. Siegbahn, H. Rensmo, *J. Phys. Chem. C* **2011**, *115*, 11996 – 12004.
[57] K. F. Jensen, H. Brandt, C. Im, J. Wilde, A. Hinsch, *Proceedings of the 28th European Photovoltaic Solar Energy Conference and Exhibition*, Paris, **2013**, 2752 – 2757.
[58] M. M. Islam, T. Okajima, S. Kojima, T. Ohsaka, *Chem. Commun.* **2008**, 5330 – 5332.
[59] a) M. I. Asghar, K. Miettunen, J. Halme, P. Vahermaa, M. Toivola, K. Aitola, P. Lund, *Energy Environ. Sci.* **2010**, *3*, 418 – 426; b) H. Matsui, K. Okada, T. Kitamura, N. Tanabe, *Sol. Energy Mater. Sol. Cells* **2009**, *93*, 1110 – 1115; c) J. Goldstein, I. Yakupov, B. Breen, *Sol. Energy Mater. Sol. Cells* **2010**, *94*, 638 – 641; d) Fujikura Technical Review: http://www.fujikura.co.jp/00/gihou/gihou38e/pdf38e/38e_11.pdf, **2009**.
[60] S. Mastroianni, A. Lanuti, T. M. Brown, R. Argazzi, S. Caramori, A. Reale, A. Di Carlo, *Appl. Phys. Lett.* **2012**, *101*, 123302 – 123304.
[61] R. Sastrawan, PhD Thesis, *Photovoltaic Modules of Dye Solar Cells*, Albert-Ludwigs University, Freiburg im Breisgau, **2006** http://www.freidok.uni-freiburg.de/volltexte/2623/pdf/Sastrawan_Photovoltaic_modules_of_dye_solar_cells_Dissertation.pdf?origin=publication_detail.
[62] K. F. Jensen, M. M. Rahman, W. Veurman, H. Brandt, C. Im, J. Wilde, A. Hinsch, J.-J. Lee, *Int. J. Photoenergy* **2013**, 696052.
[63] a) K. Miettunen, J. Halme, A.-M. Visuri, P. Lund, *J. Phys. Chem. C* **2011**, *115*, 7019 – 7031; b) S. Mastroianni, A. Lanuti, S. Penna, A. Reale, T. M. Brown, A. Di Carlo, F. Decker, *ChemPhysChem* **2012**, *13*, 2925 – 2936.
[64] C. Y. Chen, M. Wang, J. Y. Li, N. Pootrakulchote, L. Alibabaei, C. H. Ngoc-Le, J. D. Decoppet, J. H. Tsai, C. Grätzel, C. G. Wu, S. M. Zakeeruddin, M. Grätzel, *ACS Nano* **2009**, *3*, 3103 – 3109.
[65] M. Schnabel, P. Löper, M. Canino, S. A. Dyakov, M. Allegrezza, M. Bellettato, J. López-Vidrier, S. Hernández, C. Summonte, B. Garrido, P. R. Wilshaw, S. Janz, *Sol. St. Phen.* **2014**, *205 – 206*, 480 – 485.
[66] C. Cornaro, S. Bartocci, D. Musella, C. Strati, A. Lanuti, S. Mastroianni, S. Penna, A. Guidobaldi, F. Giordano, E. Petrolati, T. M. Brown, A. Reale, A. Di Carlo, *Prog. Photovoltaics* **2013**, DOI: 10.1002/pip.2426.
[67] a) T. Trupke, P. Würfel, I. Uhlendorf, I. Lauermann, *J. Phys. Chem. B* **1999**, *103*, 1905 – 1910; b) T. Trupke, S. Baumgärtner, P. Würfel, *J. Phys. Chem. B* **2000**, *104*, 308 – 312.
[68] a) M. Bokalic, U. Opara Krasovec, M. Hocevar, M. Topic in *Photovoltaic Specialists Conference (PVSC), 2012 38th IEEE*, **2012**, pp. 001507 – 001511; b) M. Berginc, U. O. Krašovec, M. Topič, *Sol. Energy Mater. Sol. Cells* **2014**, *120*, 491 – 499; c) M. Bokalič, U. O. Krašovec, M. Topič, *Prog. Photovoltaics* **2013**, *21*, 1176 – 1180.
[69] O. Bräm, A. Cannizzo, M. Chergui, *Phys. Chem. Chem. Phys.* **2012**, *14*, 7934 – 7937.
[70] M. Giustini, D. Angelone, M. Parente, D. Dini, F. Decker, A. Lanuti, A. Reale, T. Brown, A. Di Carlo, *J. Appl. Electrochem.* **2013**, *43*, 209 – 215.
[71] Data for glass production (31 kg of CO_2 per square meter of double-glazing insulation window pane) was taken from press release of the company Saint Gobain, January 2013, for the calculation. The FTO that was used as TCO was commercially spray-coated onto the hot glass in the float-glass line with little additional energy input. Also, an integrated photovoltaic generation of 3000 kWh per square meter of module area over 25 years has been assumed.

Received: November 18, 2013
Revised: January 21, 2014
Published online on ■■ ■■, 2014

ARTICLES

In situ cell concept: A review of the state of the art of dye solar cells (DSCs) evidences a broadening range of new and fundamental topics, such as novel organic dyes and perovskites. An in situ cell-manufacturing concept (see picture) that can be applied to mesoscopic-based solar cells in general is proposed. Recent results from studies on large-area, glass-frit-sealed DSC modules are reported.

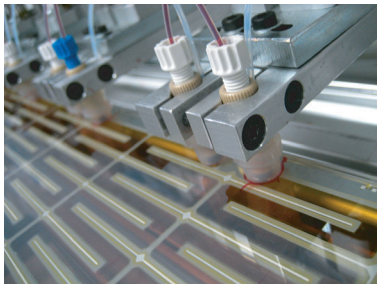

A. Hinsch, W. Veurman, H. Brandt, K. Flarup Jensen, S. Mastroianni*